Molecular Bridge Thermal Diode Enabled by Vibrational Mismatch

Yuan Dong (董源), Chenghao Diao (刁成昊), Yingru Song (宋应如), Haojia Chi (迟浩镓), David J. Singh, and Jian Lin

Phys. Rev. Applied **11**, 024043 — Published 15 February 2019

DOI: 10.1103/PhysRevApplied.11.024043

A Molecule Bridge Thermal Diode Enabled by Vibrational Mismatch

Yuan Dong[1#], Chenghao Diao[2#], Yingru Song[1], Haojia Chi[3], David J. Singh[3*], Jian Lin[1*]

[1]Department of Mechanical & Aerospace Engineering, University of Missouri, Columbia, MO 65211

[2]Department of Mechanical Engineering, Columbia University, NY 10027

[3]Department of Physics and Astronomy, University of Missouri, Columbia, MO 65211

# Authors contributed equally to this work.

* Corresponding Authors: LinJian@missouri.edu (J. L.) and singhdj@missouri.edu (D.J.S.)

Abstract

We elucidate a significant thermal rectification effect in molecule bridges (MBs) that covalently bond gold and carbon nanotubes (CNTs) by non-equilibrium molecular dynamics (MD) simulations. Remarkably, we find asymmetric heat flux across these MBs, resulting in significant thermal rectification. Thermal rectification ratios are found to decrease with the number of the MBs and increase with the lengths of CNTs, reaching a value of as high as 3.75. In addition, the calculations show that the thermal conductances vary with orientation of the crystal planes of Au, the number of molecular bridges, and the length of the CNTs. They are in a range of 40-250 MW m^{-2} K^{-1}, agreeing well with the reported experimental results. Detailed analysis suggests that the thermal rectification can be attributed to the mismatch of vibrational modes between neighboring sulfur and carbon atoms in the MBs. This discovery could provide theoretical guidance in designing molecular thermal diodes, paving new routes to potential applications in nanoscale heat manipulation, waste energy harvest, chip cooling, and molecular phononics.

Keywords: molecular bridge, thermal rectification, vibrational mismatch, MD simulation

1. Introduction

A thermal diode is an elementary device that enables sophisticated manipulation of heat, i.e. making heat flow preferentially in one direction [1-4]. It was proposed as foundation for a wide range of applications in thermal logic circuits [5], phononic computers [6], thermal regulation of buildings, and heat engines. Motivated by these many potential applications, researchers have proposed a variety of methods for constructing different types of thermal diodes for many years. A straightforward approach is to connect two materials with different temperature-dependent thermal conductivities. However, an extremely large temperature gradient is required to obtain a rectification ratio (R) of just 0.5. This is because the thermal conductivity usually has a weak temperature dependence [7, 8]. Phase change materials were also harnessed to make a thermal diode with a larger R (up to 1.20) when a relatively smaller temperature gradient is present [9]. But associated issues are the slow phase change and the limited range of working temperatures, thus hindering practical applications. Besides these traditional approaches, researchers reported other unusual methods by employing convection (thermosyphon) [10], temperature dependent electromagnetic resonances [11], magnetic field control of nanofluids [12] or thermal expansion/contraction [13, 14]. Nevertheless, all these approaches have problems, such as slow response, difficulty of system miniaturization, or complexity of system structures. An important way forward may be to use nanoscale devices and associated transport phenomena to obtain small size thermal diodes, which may enable novel phononic applications.

Recent advances in nano-materials and nanotechnology have in fact made fabrication of thermal diodes at micro/nanoscales possible, which affords new revenues to high-efficiency thermal diodes [15, 16]. In this regard, a solid state nanoscale thermal diode (SSNTD) is needed due to its potential durability, a fast response, miniaturization, and possibility for large scale integration. To fully realize these advantages, fundamentally understanding the rectification

mechanisms at the small scales becomes critical. There have been several proposed models, including those based on asymmetric geometry of nanostructures [17-22], asymmetric coupling with thermal contacts [23, 24], and asymmetric onsite potential of particles [25], and a model of one-dimension (1D) particle chains with gradient mass distribution. This latter one has been proposed to achieve *R* of several hundred [1, 25-27]. That arises because a large mass gradient can cause a large phonon mismatch and resulting asymmetry between heat flow in forward and backward directions [26]. However, this mechanism is based on an ideal model, lacking characteristics based on a real material system.

Recently, a gold (Au)-carbon nanotube (CNT) system that is chemically bonded by molecular bridges (MBs) was experimentally demonstrated [28]. It was found that the MBs significantly enhanced the interfacial thermal conductance between Au and CNTs. However, no thermal rectification was observed in that work. The reason could be the small temperature gradient applied on the systems. Given the significant mass gradients formed between Au and the MBs or inside the elements of the MBs, we hypothesize that this system could be a suitable prototype for a practical realization of the 1D mass-gradient system to achieve thermal rectification. To test this hypothesis, we used NEMD simulations to explore the possible thermal rectification effect. The results show that the interfacial thermal conductance can be significantly enhanced by these MBs. Importantly, we find that asymmetric heat flux across this system can occur, resulting in a thermal rectification ratio that can exceed 3.75. Detailed spectral analysis reveals that the rectification is mainly contributed by the vibrational mismatch between the S and its neighboring C atoms in the MBs. Interestingly, although the Au - sulfur bond has a larger mass difference, the corresponding vibrational modes are not strongly mismatched, presumably due to the coordination of Au, which is not in the 1D chain. Our study further validates the conclusion from the prior theoretical works, which show that 1D mass gradient systems would

cause vibrational mismatch for the thermal rectification, and provides a practical example. This discovery may pave the way to experimentally realizing the thermal diodes with large rectification ratios, which possess promising applications in nanoscale heat manipulation [15], waste energy harvest [29, 30], chip cooling [31], and molecular phononics [32].

2. Methods

2.1 Simulation details and model setup

NEMD simulations were implemented by the LAMMPS package [33], which are powerful tools to study the nanoscale heat transfer [34]. The simulation systems are consisted of Au, CNTs, and MBs. The lattice parameter of Au crystal is 408.72 pm. Different crystal planes were investigated to explore their effects on the interfacial thermal conductance. The Au crystals are formed of unit cells ($x \times y \times z$) with number of $6 \times 6 \times 10$, $7 \times 10 \times 10$, and $8 \times 5 \times 10$ for (1 0 0), (1 1 0) and (1 1 1) planes, respectively. This choice results in similar surface areas in x-y plane and consistently 20 atomic layers in the z direction.

An equilibrium carbon bond length (144.5 pm) of CNT obtained after relaxation of the structure was used to build the models. It is consistent with the value obtained from our previous work [35]. A unit cell of CNT with (10, 0) chirality was generated by TubeGen 3.4 [36]. Then the unit cell with a length of 433.5 pm was extended to obtain CNTs with various lengths of L_{CNT} = 10 nm, 50 nm and 100 nm for the systems. The open-ended CNT has the radius of r = 399.6 pm. Periodic boundary conditions were applied in all three Cartesian directions. In order to eliminate the interaction between periodic images, 15 nm vacuum spaces were set on the left hand side of the Au crystal and on the right hand side of the CNTs. In the simulations, an external force of F_0 = 8.26 pN was applied to the right end of a CNT in longitudinal axis direction to avoid the CNT to be pulled toward the Au crystal surface. The force was tested to ensure formation of stable peptide bonds.

2.2 Calculation on interfacial thermal conductance

The interfacial thermal conductance in both directions was calculated. To obtain the temperature profile, each system was equally divided into segments with length of 0.2 nm. The temperature of each segment was calculated using average kinetic energy of the atoms: $T_j = \frac{1}{3k_B N_j} \sum_{i \in S_j} m v_i^2$, where T_j is the local temperature of segment j, N_j is the number of atoms in the segment, m is the atomic mass, V_i is the atomic velocity, and k_B is the Boltzmann constant. The temperature drop, ΔT, across the MBs, was calculated using the edge temperature of Au and CNT at the interface by linearly fitting of temperature profiles on both sides.

In all the simulations, three main steps were applied: initialization, equilibration, and heat flux imposing. The time step is set for 0.1 fs for initialization and equilibration steps, and 0.2 fs for heat flux imposing step. First, the systems were initialized in NVT ensemble (Constant number of particles (N), volume(V) and temperature (T)) at 400 K for 0.1 ns followed by covalently bonding Au and CNT by S-Au bonds [28]. After initialization, the system is equilibrated in NVT at 300 K for 0.2 ns and then in NVE ensemble (Constant number of particles (N), volume (V) and energy (E)) for another 0.2 ns. The average Au-S bond lengths were measured to be 0.28 nm after these two steps, compared to 0.3 nm at the initialization, showing the stability of our system. Then the heat flux, Q, was applied in forward or backward directions to all systems. The heat flux was imposed following Ikeshoji and Hafskjold's method [37]. The velocities of atoms in the hot bath and the cold bath were scaled according to the energy change rate at each time step. The total momentum was kept unchanged during this process. Q is varied from 1.328 to 13.28 nJ to ensure the temperature drop, ΔT, across the Au/CNT interface in the range of 30 K to 100 K. The systems were then simulated for 2 ns until they reached the steady state, which is defined by the fluctuation of average ΔT less than 5%. Then another 6 ns simulation was used to

average the temperature profile. Consequently, the interfacial thermal conductance, K, across the MBs is given by: $K = \frac{Q}{A\Delta T}$, where $A = \pi\left(r + \delta/2\right)^2$. δ is the thickness of CNT walls, which is 0.335 nm. It is defined as the cross-section area of a CNT projected to the Au surface. Note that this definition can well reflect the thermal conductance based on the occupied surface area, which is identical to the case in experiment [28]. Several factors affecting the interfacial thermal conductance, including the Au lattice planes, MB numbers (reflecting the bond quality), and CNT lengths were studied. We also investigated the thermal rectification phenomenon by imposing reversal heat flux to these systems. In this situation, Q is set as exactly the same value in both directions to ensure the proper definition of rectification ratio. The conductance, K_+ and K_- were calculated to obtain R, which is defined as $R=K_+/K_- - 1$.

2.3 Study of vibrational properties and evolution of structures

To get more fundamental insights on the mechanism of thermal rectification in our models, the vibrational spectral density (VSD) of atoms and components from the system in both heat flux directions were calculated. The VSD were extracted from discrete Fourier transform of the velocity autocorrelation function: $D(\omega) = \int_0^\tau \langle v(0) \cdot v(t) \rangle \exp(-i\omega t)\mathrm{d}t$, where D is the spectral density at the frequency ω and $\langle v(0) \cdot v(t) \rangle$ is the correlation function of atomic velocities. In this work, the atomic velocities at two directions were collected in 0.2 ns under NVE after the systems reached the steady states. To quantify the degree of overlap of the VSD between atoms or components in the systems, the cumulative correlation factor (CCF) introduced by Li et al. [38] and Zhang et al. [39] was used to represents the match-mismatch degree of vibrational modes among them. In this work, the CCF is defined by $M_{ij}(\omega_s) = \frac{\int_0^{\omega_s} D_i(\omega) D_j(\omega) d\omega}{\int_0^{\infty} D_i(\omega) d\omega \int_0^{\infty} D_j(\omega) d\omega}$, where i and j represent individual groups of atoms, and $M(\omega_s)$ is the CCF of PDOS below a specific frequency,

ω_s, between *i* and *j*. When comparing the CCFs in each system at the two opposite directions, we normalized them by dividing $M(\omega_s)$ by $M(\infty)$.

To investigate whether the atom locations and bonding conditions contribute to the thermal rectification, we traced the average atoms positions. The pair radical distribution function (RDF) was then calculated to afford insight into structure features related to thermal rectification. The RDF is defined as $g_{ij}(L) = \frac{\mathrm{d}n_{ij}(L)}{4\pi L^2 \rho_i \mathrm{d}L}$, where L is the distance, $\mathrm{d}n_{ij}$ is the number of j^{th} type of atom at a distance between r and $r + \mathrm{d}r$ from a i^{th} type of atom, ρ is the number density of i^{th} type atoms. The peaks of RDF reflect the average bond lengths and the FWHM of corresponding peaks reflect the fluctuation amplitude of bonds, which are related to the stiffness of bonds and local temperature.[35, 40]

3. Results

3.1 Study of interfacial thermal conductance through MBs

All the NEMD simulations were based on the ReaxFF potentials [41, 42], which we have previously used to successfully predict the thermal conductivity of CNT, graphene, and 2D carbon nitride polymers [35, 40]. The parameterized ReaxFF potential is able to describe the interactions between carbon and various elements such as H, N, O, S, and Au [41]. Thus, it brings new opportunities for studying the heat transfer process at the interface of CNTs and Au bonded by the MBs (Fig. 1a). The models built here follow the previously reported experimental systems [28]. A MB (-CO-NH-CH_2–CH_2-S-) is formed by reaction of a cysteamine molecule [$NH_2(CH_2)_2SH$] with a CNT and an Au crystal. One end of the MB is bonded to the CNT which is functionalized by a carboxyl group. Thus, it can be reacted with an amine group in the cysteamine molecule to form a peptide bond (Fig. 1b). To ensure a covalent bond, the distance between Au surface and the S atom was validated to be 3 Å. The other end of the MB is bonded

to an Au crystal plane via a sulfur-Au bond (Fig. 1c). In the simulations, (1 0 0), (1 1 0) and (1 1 1) planes of the Au crystals were employed to study their effect on the thermal transport (Fig. S1 [43]). Details of system construction are given in the Methods section.

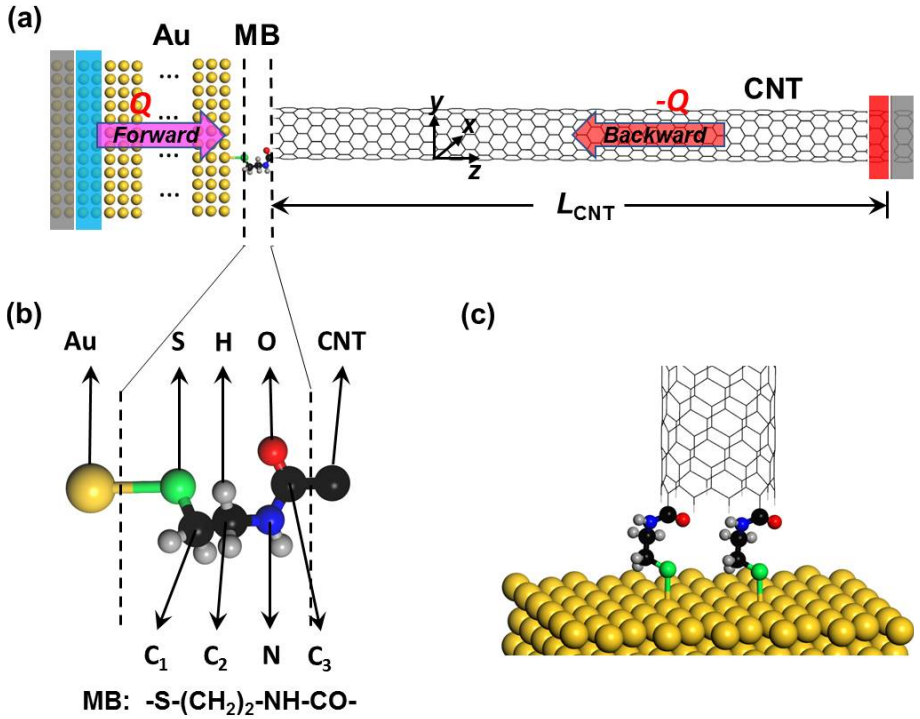

Figure 1. (a) Schematic of a simulated system consisting of Au and a CNT connected by a molecule bridge (MB); heat flows across the MB from Au to the CNT in the forward direction or from the CNT to Au in the backward direction. Red and blue areas denote the heat bath regions; the gray shadow areas on both ends denote the boundary of the system. (b) Detailed view of a MB (-S-$(CH_2)_2$-NH-CO-). One end of the MB is bonded to a CNT through a peptide bond. The other end is bonded to Au lattice through S-Au bond. (c) A schematic of Au/CNT interfaced via two MBs.

We first studied the interfacial thermal conductance (K) on all of the constructed Au/CNT systems, which have different Au crystallographic lattice planes, CNT lengths, and different

numbers of MBs. Fig. 2a shows a representative temperature profile of one of these systems. The system consists of CNT with 100 nm, one MB, and Au crystal with (1 0 0) plane. A temperature drop, ΔT, can be used to calculate the interfacial thermal conductance (see Methods). Simulation on a control system of Au/CNTs without MBs results in an infinite ΔT, indicating zero K. With just a single MB, ΔT is significantly reduced to ~60 K with a heat flux Q=0.032 eV/ps=5.12 nJ, resulting in an interfacial thermal conductance of 85 MW m^{-2} K^{-1} (See Methods 2.2). As the number of the MB increases, the calculated K is greatly enhanced (Fig. 2b), as may be expected. For instance, it increases from 85 MW m^{-2} K^{-1} to 210 MW m^{-2} K^{-1} when the number of MB increases from one to three MBs in the systems with the 100 nm CNTs. This conclusion agrees well with the experiment [28]. and corresponds simply to the statement that K strongly depends on the bonding quality, in other words, the number of real bonds. It can be varied from 30 MW m^{-2} K^{-1} for poor bonding to 360 MW m^{-2} K^{-1} for very good bonding [28]. Moreover, Fig. 2b shows that K is also greatly affected by the CNT lengths. As the length of CNTs for the systems consisting of 1 MB, 2 MBs and 3 MBs increases from 10 nm to 100 nm, K is increased by 110%, 60% and 35%, respectively. This increasing K with the length reflects the one-dimensional (1D) nature of the CNTs. Chen et. al. demonstrated that in a superlattice K is not merely an intrinsic property of the interface but also positively correlated to the phonon mean free paths (MFPs) of materials in the interfaces [44]. In the ballistic thermal transport of 1D nanosystems, the effective MFPs are greatly determined by the lengths of CNT [21, 45]. For example, based on the Matthiessen law for diffusive-ballistic transport [45, 46], the effective MFP of CNT, λ_{eff}, can be expressed as $1/\lambda_{\text{eff}} = 1/\lambda_0 + 1/L$, where λ_0 is the intrinsic MFP and L is the length of CNT. Our previous MD work showed the intrinsic MFP of CNT is 442 nm based on the current potential we adopted [35]. The resultant effective MFPs for 10 nm, 50 nm and 100 nm CNT are 9.78 nm, 44.9 nm, 81.5 nm, respectively. Thus a longer CNT leads to a longer MFP, which is beneficial to

the heat transfer through the interfaces. The results provide another example of nanoscale systems showing the nonlocal behavior of interface thermal conductance [47]. Fig. 2c shows that the particular crystallographic plane of the Au also affects *K*. The system built with (1 0 0) Au lattice plane has the highest *K* of ~ 165 MW m^{-2} K^{-1}, which is 44% higher than that of system built with the (1 1 1) Au lattice plane. In the following simulations, unless specifically indicated, all the results are reported based on systems built on the (1 0 0) Au lattice plane.

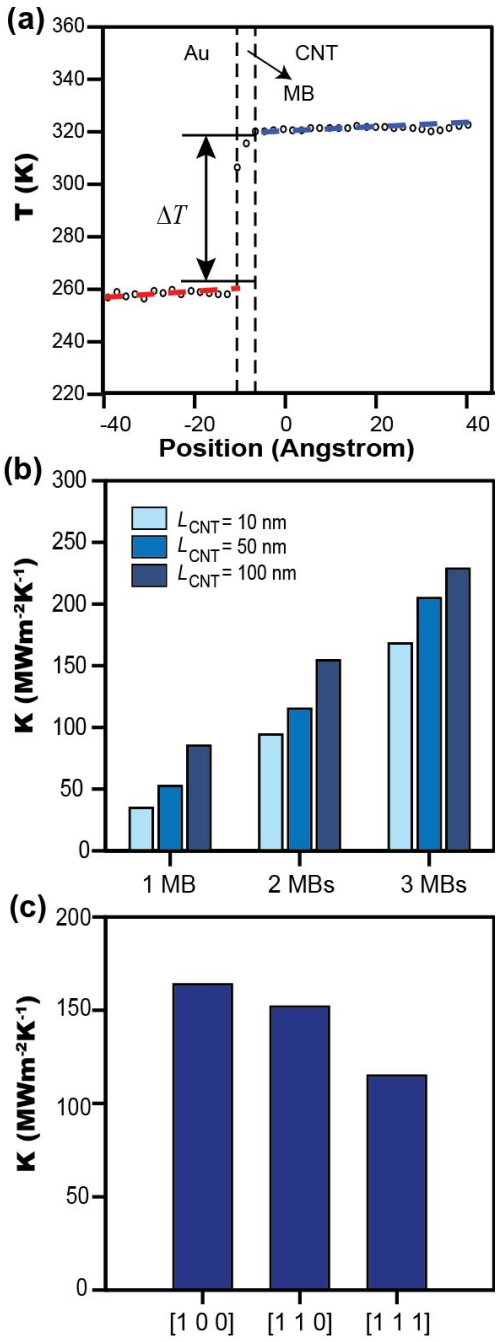

Figure 2. (a) A representative temperature profile for a system built with (1 0 0) Au crystallographic lattice plane, a single MB, and a CNT with L_{CNT} = 100 nm. (b) Interfacial thermal conductance as a function of number of the MBs and lengths of the CNT. (c) Interfacial thermal conductance as a function of Au lattice planes for systems built with three MBs and CNTs with L_{CNT} = 10 nm.

3.2 Thermal rectification

To investigate thermal rectification effect of the Au-MB-CNT systems, we performed NEMD simulations by applying heat flux in two opposite directions. Fig. 3a-b show the obtained K from systems built with 10 nm and 50 nm CNTs and 1, 2, and 3 MBs in the forward and backward heat flux directions. We find that K for the forward direction (K_+) are much larger than those for the backward direction (K_-) for systems with the same number of the MBs, showing the thermal rectification effect. Both forward and backward K increase with the number of the MBs, but R decreases with increasing number of the MBs. For example, it is reduced from 1.2 for the system with one MB to 0.59 for the system with three MBs (Fig. 3a). As the length of the CNT increases from 10 nm to 50 nm, R increases to 3.75 for the system with one MB and 3.15 for the system with three MBs, respectively. It is intriguing to explore whether this trend still holds for more MBs, or larger CNT sizes. These effects are to be studied in future work to provide more systematic and comprehensive understanding on these phenomena. Recently, Ma and Tian simulated tapered bottlebrush polymer by MD and obtained R with a maximum value of 0.7 [21]. Similar length dependent R was observed in their work, which was attributed to the ballistic transport. Considering that the models are based on experimentally synthesized systems, our simulation results are very promising for realization of future practical thermal diodes.

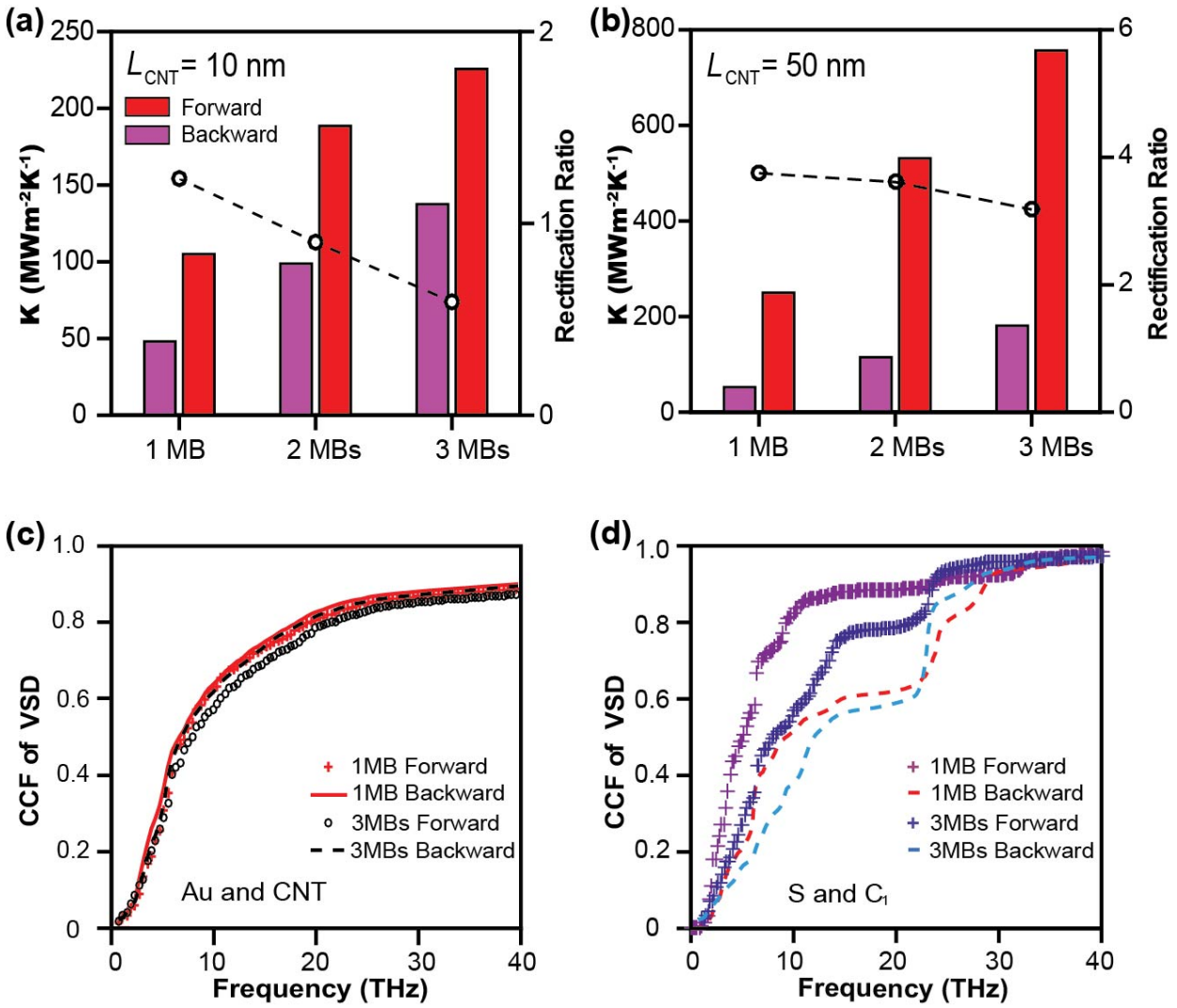

Figure 3. (a, b) Forward and backward interfacial thermal conductance and rectification ratio, *R*, of systems built with the same CNT but different numbers of MBs; (a) L_{CNT} = 10 nm, (b) L_{CNT} = 50 nm. Cumulative correlation factor (CCF) of VSD (c) between Au and CNT, (d) between S and C_1 atoms (see Fig. 1b) for systems built with L_{CNT} = 10 nm CNTs and 1 MB and 3 MBs, respectively.

Vibrational behavior can be described by spectral functions determined from the velocity autocorrelation. Here we use a local vibrational spectral density (VSD), extracted from the

Fourier transform of the velocity autocorrelation function, $D(\omega)=\int_0^{\tau}\langle v(0)\cdot v(t)\rangle \exp(-i\omega t)\,\mathrm{d}t$, where D is the spectral density at the frequency ω and $\langle v(0)\cdot v(t)\rangle$ is the correlation function of atomic velocities. This is convenient because we are dealing with non-diffusive transport, where there is a steady state but a local equilibrium cannot be assumed. Theory indicates that the mismatch of vibrational modes between two lattices or atoms can cause thermal rectification.[1, 3, 26] In a molecular system, different atomic weight of each atom or component may cause mismatch of their vibrational modes. For instance, in our simulated systems, in the forward heat flux direction (Au to CNTs), the atomic weights of main atoms–Au (196)-S (32)-C (12)– decrease in sequence in a very short distance (~5 Å), which leads to a significant mass gradient. To test the hypothesis that such a mass gradient can result in a thermal rectification effect, we calculated the local VSD of the different components in the systems, including Au lattices, CNT, and S, C, N, O atoms in the MBs in the forward and backward heat flux directions. The VSD for hydrogen atoms are not shown. We denoted the three C atoms in the MBs as C_1, C_2, and C_3 (Fig. 1b). In contrast to previous work that qualitatively compares the phonon density of states (PDOS) [26, 48]. we used a cumulative correlation factor (CCF) [39] to quantify the degree of overlap between the VSD of two components or two atoms in the systems when the heat flows in opposite directions. Here, the CCF is calculated following the method proposed by Li et al. [38] and Zhang et al.[39] (see Methods). Since the thermal transport is mainly contributed by the low-frequency modes [45]. a smaller CCF at low frequency range means a larger mismatch, resulting in a lower interfacial thermal conductance (K) in that direction. Thus, a larger difference of CCFs in the forward and backward heat flux directions indicates a larger difference in K, leading to a larger thermal rectification ratio.

Here we calculated the CCFs between all possible configurations of atoms in the systems to elucidate the dominant rectification sites in the MBs. As shown in Fig. 3c, the CCFs of the local

VSD between Au and CNT in the systems with one and three MBs are quite similar in the forward and backward directions, showing a small degree of mismatch of vibrational modes between them. This excludes attribution of the thermal rectification to vibrational mismatch of Au and CNT. Besides, we also calculated individual CCFs of the local VSD between Au and S, S and C_1, C_2 and N, N and C_3, C_3 and CNT atoms (Fig. S2-S4 [43]). They all show little difference in the forward and backward directions. Surprisingly, the CCFs between S atom and C_1 atom in opposite heat flux directions have large differences (Fig. 3d). The CCFs in the forward direction are higher than those in the backward direction, indicating a better vibrational matching in the forward direction than that in the backward direction. This explains why the interfacial thermal conductance in the forward direction is larger than that in the backward direction, leading to thermal rectification.

The local VSDs are also plotted (Fig. S5 and S6 [43]). Fig. S5 confirms that the VSD between Au and CNT does not change much with the heat flux direction. However, the overlap of the VSD between S and C_1 is clearly seen to be larger in the forward heat flux direction than in the opposite direction (Fig. S6). The different CCFs of local VSD between S and C_1 are caused by a large gradient of atomic masses in the MBs. Moreover, the difference of the CCFs in the system with 1 MB is larger than that of the system with 3 MBs, which is consistent with the results showing that the rectification ratio in the 1-MB system is larger than that in the 3-MBs system (Fig. 3a, b). These results validate the hypothesis that the thermal rectification is due to the mismatch of vibrational modes between atoms in a single MB. It is intriguing that the Au and S have quite different atomic weights, but they contribute little to the thermal rectification. In all previous theories [26, 27], the mass gradient generates thermal rectification only in 1D systems. In this simulation, the Au atoms are in a form of a bulk crystal plane. Therefore, the mass

gradient between S and C_1 atoms in the 1D chain contributes to the thermal rectification while the Au-S bond does not.

Another cause of the vibrational mismatch when the forward and backward heat fluxes are applied could arise from the change in atom locations, i.e. thermally induced structural change. In this regard, we also calculated pair radical distribution function (RDF) of S-C_1 atoms in the forward and backward directions. This reflects the key structural information of MBs during the heat transport. The calculations were based on the systems with 10 nm-CNT and 1-, 2-, 3-MBs (Fig. 4). The peak positions represent the equilibrium bond lengths of S-C_1. The average bond lengths are barely changed. As summarized in Table S1 and S2, the S-C_1 distances change less than 0.01 Å between heat fluxes in the forward or backward directions. Therefore, we conclude that the rectification cannot be attributed to the structural change of the MBs. Nevertheless, we found an observable change of full width at half maximum (FWHM) for the peaks related to the S and C_1 atoms. The peak appearing at around 0.2 nm corresponds to the S-C_1 bonds. The FWHM of this peak in forward condition is smaller than that in the backward condition by 17%, 27% and 20% for the systems with 1 MB, 2 MBs and 3 MBs, respectively. In contrast, the Au-S bonds do not show such an apparent peak shift or variations in FWHM in different heat flux directions (Fig. S7 [43]). This is consistent with the different VSD for the different heat flow directions and in particular the local potential energy reflected in the FWHM is different, and therefore the local kinetic energy must also be different.

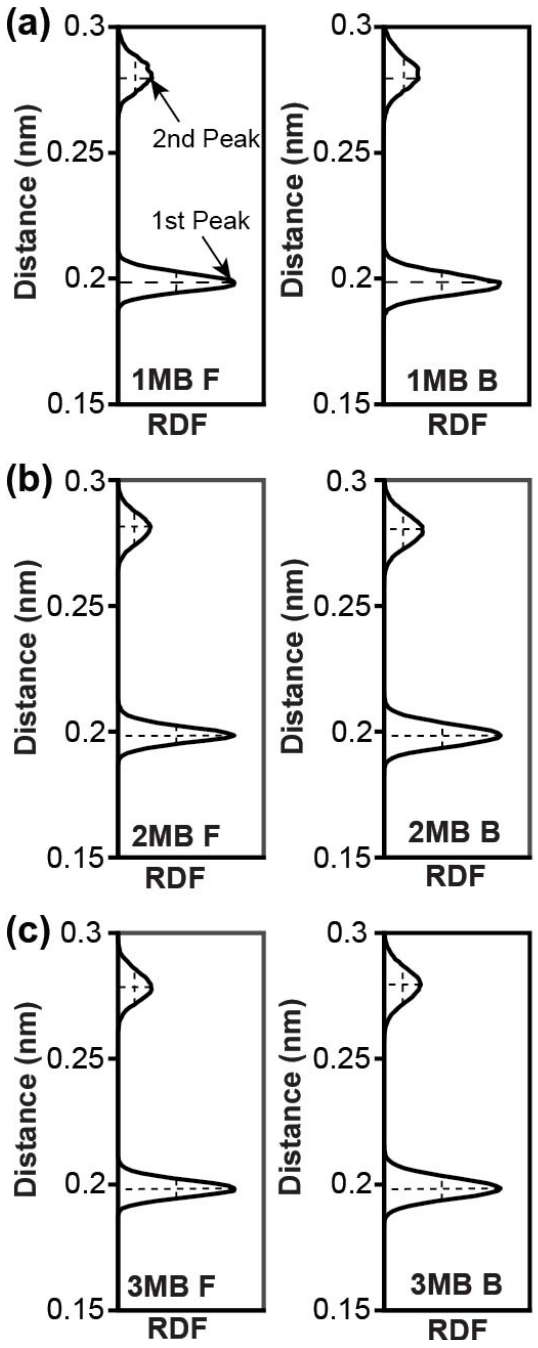

Figure 4. Pair radical distribution function (RDF) between S and C_1 atoms in systems with L_{CNT} = 10 nm CNTs and (a) 1MB, (b) 2MBs, (c) 3MBs. The left column shows the RDF in forward (F) direction and the right column shows the RDF in the backward (B) direction.

4. Conclusion

We used the NEMD to investigate the thermal transport across the Au-CNT interfaces coupled by molecular bridges. We found that the interface thermal conductance depends on the Au crystallographic orientation, increases with the number of molecular bridges and the length of the CNTs. Importantly, we find significant thermal rectification in these systems. These phenomena can be well explained by a mass gradient model, which can explain the vibrational mismatch of the S-C_1 bond in the MB in the forward and backward heat flux directions. We demonstrate the contribution to the thermal rectification by quantification of the degree of mismatch of the local vibrational spectral densities (VSDs). Finally, the change of FWHM of S and C_1 atoms in the calculated RDFs further validates such conclusion from a different perspective. We envision that our work would stimulate further experimental work on thermal rectification in nanoscale MB systems. In this work, only the phonon contribution to thermal transport was considered due to the limitation of MD simulation. In real devices, the electron could also contribute to the thermal transport across the system and affect the thermal rectification ratio. This issue is to be studied in future work using experiments or ab initio MD simulations which include the contribution of electrons.

Acknowledgements

J.L. acknowledges financial support from University of Missouri-Columbia start-up fund, NASA Missouri Space Consortium (Project: 00049784), Department of Energy National Energy Technology Laboratory (Award Number: DE-FE0031645), and United States Department of Agriculture (Award number: 2018-67017-27880). The computations were performed on the HPC resources at the University of Missouri Bioinformatics Consortium (UMBC), supported in part

by NSF (Award number: 1429294). Work of D.S. was supported by the U.S. Department of Energy, Office of Science, Basic Energy Sciences through the MAGICS center, award DE-SC0014607.

References

[1] B. Li, L. Wang, and G. Casati, Thermal diode: Rectification of heat flux, Phys. Rev. Lett. **93**, 184301 (2004).

[2] C. Chang, D. Okawa, A. Majumdar, and A. Zettl, Solid-state thermal rectifier, Science **314**, 1121 (2006).

[3] N. Li, J. Ren, L. Wang, G. Zhang, P. Hänggi, and B. Li, Colloquium: Phononics: Manipulating heat flow with electronic analogs and beyond, Rev. Mod. Phys. **84**, 1045 (2012).

[4] G. Wehmeyer, T. Yabuki, C. Monachon, J. Wu, and C. Dames, Thermal diodes, regulators, and switches: Physical mechanisms and potential applications, Applied Physics Reviews **4**, 041304 (2017).

[5] O.-P. Saira, M. Meschke, F. Giazotto, A. M. Savin, M. Mttnen, and J. P. Pekola, Heat transistor: Demonstration of gate-controlled electronic refrigeration, Phys. Rev. Lett. **99**, 027203 (2007).

[6] L. Wang, and B. Li, Thermal logic gates: computation with phonons, Phys. Rev. Lett. **99**, 177208 (2007).

[7] C. Dames, Solid-state thermal rectification with existing bulk materials, J. Heat Transfer **131**, 061301 (2009).

[8] W. Kobayashi, Y. Teraoka, and I. Terasaki, An oxide thermal rectifier, Appl. Phys. Lett. **95**, 171905 (2009).

[9] T. Zhang, and T. Luo, Giant thermal rectification from polyethylene nanofiber thermal diodes, Small **11**, 4657 (2015).

[10] Y. Lee, and U. Mital, A two-phase closed thermosyphon, Int. J. Heat Mass Transfer **15**, 1695 (1972).

[11] C. R. Otey, W. T. Lau, and S. Fan, Thermal rectification through vacuum, Phys. Rev. Lett. **104**, 154301 (2010).

[12] J. B. Puga, B. D. Bordalo, D. J. Silva, M. M. Dias, J. H. Belo, J. P. Araújo, J. C. Oliveira, A. M. Pereira, and J. Ventura, Novel thermal switch based on magnetic nanofluids with remote activation, Nano energy **31**, 278 (2017).

[13] C. Y. Tso, and C. Y. Chao, Solid-state thermal diode with shape memory alloys, Int. J. Heat Mass Transfer **93**, 605 (2016).

[14] P. R. Gaddam, S. T. Huxtable, and W. A. Ducker, A liquid-state thermal diode, Int. J. Heat Mass Transfer **106**, 741 (2017).

[15] M. Maldovan, Sound and heat revolutions in phononics, Nature **503**, 209 (2013).

[16] E. Pop, Energy dissipation and transport in nanoscale devices, Nano Research **3**, 147 (2010).

[17] J. Hu, X. Ruan, and Y. P. Chen, Thermal conductivity and thermal rectification in graphene nanoribbons: a molecular dynamics study, Nano Lett. **9**, 2730 (2009).

[18] X. Yang, D. Yu, B. Cao, and A. C. To, Ultrahigh Thermal Rectification in Pillared Graphene Structure with Carbon Nanotube–Graphene Intramolecular Junctions, ACS Appl. Mater. Interfaces **9**, 29 (2016).

[19] X. Yang, D. Yu, and B. Cao, Giant Thermal Rectification from Single-Carbon Nanotube–Graphene Junction, ACS Appl. Mater. Interfaces **9**, 24078 (2017).

[20] H. Wang, S. Hu, K. Takahashi, X. Zhang, H. Takamatsu, and J. Chen, Experimental study of thermal rectification in suspended monolayer graphene, Nat. Commun. **8**, 15843 (2017).

[21] H. Ma, and Z. Tian, Significantly High Thermal Rectification in an Asymmetric Polymer Molecule Driven by Diffusive versus Ballistic Transport, Nano Lett. **18**, 43 (2018).

[22] N. Yang, G. Zhang, and B. Li, Thermal rectification in asymmetric graphene ribbons, Appl. Phys. Lett. **95**, 033107 (2009).

[23] L.-A. Wu, and D. Segal, Sufficient conditions for thermal rectification in hybrid quantum structures, Phys. Rev. Lett. **102**, 095503 (2009).

[24] J. Lee, V. Varshney, A. K. Roy, J. B. Ferguson, and B. L. Farmer, Thermal rectification in three-dimensional asymmetric nanostructure, Nano Lett. **12**, 3491 (2012).

[25] M. Terraneo, M. Peyrard, and G. Casati, Controlling the energy flow in nonlinear lattices: a model for a thermal rectifier, Phys. Rev. Lett. **88**, 094302 (2002).

[26] N. Yang, N. Li, L. Wang, and B. Li, Thermal rectification and negative differential thermal resistance in lattices with mass gradient, Phys. Rev. B **76**, 020301 (2007).

[27] E. Pereira, Requisite ingredients for thermal rectification, Physical Review E **96**, 012114 (2017).

[28] S. Kaur, N. Raravikar, B. A. Helms, R. Prasher, and D. F. Ogletree, Enhanced thermal transport at covalently functionalized carbon nanotube array interfaces, Nat. Commun. **5**, 3082 (2014).

[29] B. Xu, L. Liu, H. Lim, Y. Qiao, and X. Chen, Harvesting energy from low-grade heat based on nanofluids, Nano Energy **1**, 805 (2012).

[30] M. López-Suárez, G. Abadal, L. Gammaitoni, and R. Rurali, Noise energy harvesting in buckled BN nanoribbons from molecular dynamics, Nano Energy **15**, 329 (2015).

[31] A. L. Moore, and L. Shi, Emerging challenges and materials for thermal management of electronics, Materials Today **17**, 163 (2014).

[32] J. M. Tour, Molecular electronics. Synthesis and testing of components, Acc. Chem. Res. **33**, 791 (2000).

[33] S. Plimpton, Fast parallel algorithms for short-range molecular dynamics, J. Comput. Phys. **117**, 1 (1995).

[34] H. Bao, J. Chen, X. Gu, and B. Cao, A Review of Simulation Methods in Micro/Nanoscale Heat Conduction, ES Energy & Environment **1**, 16 (2018).

[35] C. Diao, Y. Dong, and J. Lin, Reactive force field simulation on thermal conductivities of carbon nanotubes and graphene, Int. J. Heat Mass Transfer **112**, 903 (2017).

[36] D. J. D. J. T. Frey, in *University of Delaware, Newark DE,*2011).

[37] T. Ikeshoji, and B. Hafskjold, Non-equilibrium molecular dynamics calculation of heat conduction in liquid and through liquid-gas interface, Molecular Physics **81**, 251 (1994).

[38] B. Li, J. H. Lan, and L. Wang, Interface thermal resistance between dissimilar anharmonic lattices, Phys. Rev. Lett. **95**, 104302 (2005).

[39] L. Zhang, and L. Liu, Polymeric Self-Assembled Monolayers Anomalously Improve Thermal Transport across Graphene/Polymer Interfaces, ACS applied materials & interfaces **9**, 28949 (2017).

[40] Y. Dong, M. Meng, M. M. Groves, C. Zhang, and J. Lin, Thermal conductivities of two-dimensional graphitic carbon nitrides by molecule dynamics simulation, Int. J. Heat Mass Transfer **123**, 738 (2018).

[41] S. Monti, V. Carravetta, and H. Ågren, Simulation of gold functionalization with cysteine by reactive molecular dynamics, J. Phys. Chem. Lett. **7**, 272 (2016).

[42] A. C. Van Duin, S. Dasgupta, F. Lorant, and W. A. Goddard, ReaxFF: a reactive force field for hydrocarbons, J. Phys. Chem. A **105**, 9396 (2001).

[43] See Supplemental Material at [URL will be inserted by publisher] for details.

[44] G. Chen, Thermal conductivity and ballistic-phonon transport in the cross-plane direction of superlattices, Phys. Rev. B **57**, 14958 (1998).

[45] Y. Dong, B.-Y. Cao, and Z.-Y. Guo, Ballistic–diffusive phonon transport and size induced anisotropy of thermal conductivity of silicon nanofilms, Physica E: Low-dimensional Systems and Nanostructures **66**, 1 (2015).

[46] Y. Dong, Dynamical analysis of non-Fourier heat conduction and its application in nanosystems (Springer, 2015).

[47] D. Tzou, Nonlocal behavior in phonon transport, Int. J. Heat Mass Transfer **54**, 475 (2011).

[48] C. Si, X.-D. Wang, Z. Fan, Z.-H. Feng, and B.-Y. Cao, Impacts of potential models on calculating the thermal conductivity of graphene using non-equilibrium molecular dynamics simulations, Int. J. Heat Mass Transfer **107**, 450 (2017).